



Smoothing Algorithms for Mean-Flow Extraction in Large-Eddy Simulation of Complex Turbulent Flows

A. Cahuzac, J. Boudet

LMFA - École Centrale de Lyon - Université de Lyon - CNRS

*36 avenue Guy de Collongue, 69134 Ecully Cedex, France**

P. Borgnat, E. Lévêque

Laboratoire de Physique - ENS de Lyon - Université de Lyon - CNRS

46 allée d'Italie, 69364 Lyon Cedex 07, France[†]

Abstract

Based on physical arguments, the importance of separating the mean flow (in the statistical sense) from turbulence in the modeling of the subgrid-scale eddy-viscosity is emphasized. Therefore, two distinct smoothing (in time) algorithms are proposed to estimate the mean flow as the simulation progresses. Namely, an exponentially-weighted moving average (or exponential smoothing) and an adaptive low-pass Kalman filter. These algorithms highlight the longer-term evolution or cycles of the flow but erase short-term fluctuations. Indeed, it is our assumption that the mean flow may be approximated as the low-frequency component of the velocity field and that the turbulent part of the flow adds itself to this “unsteady mean”. The cut-off frequency separating these two components is fixed according to some characteristic time-scale of the flow in the exponential smoothing, but inferred dynamically from the recent history of the flow in the Kalman filter. In practice, these two algorithms are implemented in large-eddy simulations that rely on a *shear-improved Smagorinsky model*, in which the magnitude of mean-flow rate of strain is subtracted from the magnitude of the instantaneous rate of strain in the subgrid-scale eddy-viscosity. Two test-cases have been investigated: a turbulent plane-channel flow ($Re_w = 395$) and the flow past a circular cylinder in the sub-critical turbulent regime ($Re_D = 4.7 \times 10^4$). Comparisons with direct numerical simulation and experimental data demonstrate the good efficiency of the whole modeling, which allows us to address non-homogeneous unsteady configurations without adding significant complication and computational cost to the standard Smagorinsky model. From a computational viewpoint, this modeling deserves interest since it is entirely local in space. It is therefore adapted for parallelization and convenient for boundary conditions. Another major advantage is that it does not call for any ad-hoc parameter.

The following article has been submitted to *Physics of Fluids*. After it is published, it will be found at <http://pof.aip.org>.

*Electronic address: adrien.cahuzac@ec-lyon.fr, jerome.boudet@ec-lyon.fr

†Electronic address: pierre.borgnat@ens-lyon.fr, emmanuel.leveque@ens-lyon.fr

keywords: Large-eddy simulation, non-homogeneous turbulence, unsteady flows, exponentially-weighted moving average, Kalman filter.

I. CONTEXT AND MOTIVATIONS

Large-eddy simulation (LES) is a promising technique that offers an affordable means for the numerical simulation of turbulent flows [15, 27]. Unlike the Reynolds-averaged Navier-Stokes (RANS) methods commonly used in the industry, LES gives a direct representation of the large-sized turbulent eddies and their dynamics. It is therefore expected to provide a better description of turbulence impacts. LES has already demonstrated its capabilities in computations of academic *building-block* flows, however, further progress is still required to address realistic, more complex configurations [24]. The present work aims at improving this situation. Our guideline is to develop numerical modeling that remains as simple as possible in its formulation but captures the “basic physics”, therefore offering an interesting compromise between accuracy and computational cost.

Turbulence that occurs in nature, or in engineering flows, is usually not, even approximatively, homogeneous. There are frequent variations of the mean velocity with position (and time in unsteady configurations). In the following, the general framework of LES is briefly recalled and physical arguments are brought forward to justify the importance of the mean gradients in the modeling of the subgrid-scale (SGS) eddy-viscosity.

LES is rooted in the idea to discretize the flow on a grid whose resolution is coarse compared to the size of the smallest turbulent eddies. Therefore, only the large-sized eddies are represented numerically. This is justifiable since the large-sized eddies contains most of the kinetic energy and their strength make them the efficient carriers of momentum, heat, mass, etc. On the contrary, the small-sized eddies are mainly responsible for dissipation and contribute little to transport. Conceptually, the solution of a LES is expected to represent the flow variables filtered over a “filter window” whose characteristic width corresponds to the grid resolution. These filtered variables are solutions of the flow equations supplemented by terms accounting for the action of the (unresolved) subgrid-scale (SGS) fluctuations on the grid-scale dynamics [36]. These additional terms need to be modeled in order to close the governing equations, which constitutes a major difficulty in the case of complex turbulent flows.

In the present study, primarily devoted to weakly-compressible aerodynamics, the relevant flow variables are ρ , $\rho \mathbf{u}$ and ρe_t referring respectively to the mass, the momentum and the total energy of the fluid per unit volume. The related filtered variables are $\bar{\rho}$, $\bar{\rho \mathbf{u}} \equiv \bar{\rho} \tilde{\mathbf{u}}$ and $\bar{\rho e_t} \equiv \bar{\rho} \tilde{e_t}$, where the overbar refers to the grid filter operator and the tilde is the Favre operator ($\tilde{q} = \overline{\rho q} / \bar{\rho}$). The filtered flow equations express as

$$\frac{\partial \bar{\rho}}{\partial t} + \frac{\partial (\bar{\rho} \tilde{u}_j)}{\partial x_j} = 0 \quad (1)$$

$$\frac{\partial (\bar{\rho} \tilde{u}_i)}{\partial t} + \frac{\partial (\bar{\rho} \tilde{u}_i \tilde{u}_j)}{\partial x_j} = -\frac{\partial \bar{P}}{\partial x_i} + \frac{\partial \bar{\tau}_{ij}}{\partial x_j} + \frac{\partial \Pi_{ij}^{\text{sgs}}}{\partial x_j} \quad (2)$$

$$\frac{\partial (\bar{\rho} \tilde{e}_t)}{\partial t} + \frac{\partial ((\bar{\rho} \tilde{e}_t + \bar{P}) \tilde{u}_j)}{\partial x_j} = \frac{\partial (\tilde{u}_i (\bar{\tau}_{ij} + \Pi_{ij}^{\text{sgs}}))}{\partial x_j} + \frac{\partial}{\partial x_j} \left(\bar{\lambda} \frac{\partial \tilde{T}}{\partial x_j} \right) - \frac{\partial \Theta_j^{\text{sgs}}}{\partial x_j} \quad (3)$$

Implicit summation on repeated indexes is used. The fluid is air, considered as Newtonian with constant dynamic viscosity $\bar{\mu} = 1.8 \cdot 10^{-5} \text{ kg} \cdot \text{m}^{-1} \cdot \text{s}^{-1}$:

$$\bar{\tau}_{ij} = \bar{\mu} \left(\frac{\partial \tilde{u}_i}{\partial x_j} + \frac{\partial \tilde{u}_j}{\partial x_i} - \frac{2}{3} \frac{\partial \tilde{u}_k}{\partial x_k} \delta_{ij} \right), \quad (4)$$

and constant thermal conductivity $\bar{\lambda} = 2.54 \cdot 10^{-2} \text{ W} \cdot \text{m}^{-1} \cdot \text{K}^{-1}$. Air is assumed to behave as a perfect gas, thus following

$$\bar{P} = r \bar{\rho} \tilde{T} \quad \text{with } r = 287 \text{ J} \cdot \text{kg}^{-1} \cdot \text{K}^{-1}, \quad (5)$$

where P is the pressure and T is the temperature. The ratio of specific heats (at constant pressure and volume) is fixed at $\gamma = C_p/C_v = 1.4$. The SGS stress tensor (Π_{ij}^{sgs}) and the SGS heat current (Θ_j^{sgs}) encompass the exchanges of momentum and heat with the SGS motions. A common thread in simpler models is to assume that these terms are essentially responsible for a diffusive transport at grid scale. This assumption yields

$$\Pi_{ij}^{\text{sgs}} = \mu_{\text{sgs}} \left(\frac{\partial \tilde{u}_i}{\partial x_j} + \frac{\partial \tilde{u}_j}{\partial x_i} - \frac{2}{3} \frac{\partial \tilde{u}_k}{\partial x_k} \delta_{ij} \right) \quad \text{and} \quad \Theta_j^{\text{sgs}} = \frac{-\mu_{\text{sgs}} C_p}{\text{Pr}_{\text{sgs}}} \times \frac{\partial \tilde{T}}{\partial x_j}, \quad (6)$$

where μ_{sgs} represents a SGS eddy-viscosity and $\text{Pr}_{\text{sgs}} = 0.9$ may be interpreted as a fixed SGS Prandtl number [25]. Unlike the molecular viscosity, the eddy-viscosity is a property of the flow but not of the fluid. It is therefore expected to depend explicitly on flow variables and the local grid spacing.

In practice, the eddy-viscosity is primarily intended to ensure the correct drain of kinetic energy from the resolved to the unresolved turbulent scales. Tackling this problem from a

deterministic viewpoint is mainly out of reach [18]. A statistical approach is rather adopted and an expression of the eddy-viscosity is sought on the basis of statistical hypotheses made on the SGS turbulent scales [8]. Along this line, physical arguments are now provided to defend the importance of mean-flow gradients in the SGS properties.

Despite the non-homogeneous nature of turbulent flows, it is commonly thought that the small-scale properties of turbulence should be considered as locally homogeneous (and isotropic). This hypothesis relies on the idea that small-sized eddies adjust themselves via strong non-linear interactions in which all statistical information about the large-scale inhomogeneities is lost. This is the classical phenomenology of the Kolmogorov's theory [9]. Within this picture, it is implicitly assumed (but often forgotten) that the size of the turbulent eddies should be small compared to the length-scale associated with the mean-velocity gradients, which is

$$L_s \sim \frac{u'}{\mathcal{S}}, \quad (7)$$

where $u' \equiv \sqrt{\langle |\mathbf{u}'|^2 \rangle}$ and $\mathcal{S} \equiv \sqrt{|\nabla \langle \mathbf{u} \rangle|^2}$ denote the characteristic amplitudes of the fluctuating velocity and of the mean-velocity gradient, respectively. Here, angular brackets *a priori* refer to an ensemble (statistical) average and the fluctuating velocity arises from the Reynolds decomposition: $\mathbf{u} = \mathbf{u}' + \langle \mathbf{u} \rangle$. The characteristic scale (7) is obtained by equalling the time-scale associated with the mean-velocity gradient (characteristic of the mean-flow distortion) and the turn-over time of turbulent eddies of size ℓ (characteristic of turbulent interactions at scale ℓ). That is, $1/\mathcal{S} \sim \varepsilon^{-1/3} \ell^{2/3}$ for $\ell = L_s$, according to Kolmogorov's theory [9]. From the averaged Navier-Stokes equations, the mean dissipation rate (per unit mass) $\varepsilon = -\langle u'_i u'_j \rangle \times \partial \langle u_i \rangle / \partial x_j \sim u'^2 \mathcal{S}$, which finally yields $L_s \sim u' / \mathcal{S}$ or, equivalently, $L_s \sim \sqrt{\varepsilon / \mathcal{S}^3}$ [32]. Note that the previous reasoning relies on dimensional arguments that ignore dimensionless factors. In that sense, the symbol “ \sim ” should be understood as “is of the order of”. In the jargon of fluid mechanics, \mathcal{S} is usually referred to as the shear and L_s is the shear length-scale. The shear is often expressed as

$$\mathcal{S} = \sqrt{2 \langle S_{ij} \rangle \langle S_{ij} \rangle}$$

where $\langle S_{ij} \rangle$ is the rate-of-strain tensor of the mean flow.

Turbulent eddies of size smaller than L_s evolve rapidly enough and are insensitive to the mean-flow distortion: the mean flow acts principally to convect these eddies without significantly stretching them. On the contrary, turbulent eddies of size larger than L_s have

no time to adjust dynamically while they are distorted by the mean-flow gradients. Termed differently, the shear length-scale L_s isolates the problem of the self-interaction of fluctuating velocities, at scales $\ell < L_s$, from the problem of the interaction of the fluctuating velocity with the mean-flow velocity, at scales $\ell > L_s$. This feature is of great importance in the context of LES, as it implies the statistical properties of the SGS motion (and therefore the nature of the SGS eddy-viscosity) should differ depending on whether the grid resolution Δ is locally smaller, or larger, than the shear length-scale L_s . Therefore, it is desirable to account explicitly for the mean-flow gradients in the modeling of the SGS eddy-viscosity, also the canonical assumption of homogeneous turbulence (which ignores the mean-flow inhomogeneities: $\mathcal{S} \simeq 0$ and $L_s \simeq \infty$) should be abandoned. This is particularly relevant for high-Reynolds-number flows, when the resolution of the simulation is almost comparable to the large scales of the flow. These features naturally call for a generic procedure to estimate numerically the mean flow and compute the SGS eddy-viscosity as the LES progresses. This is the main concern of the present study, which will be developed in section II. Practical implementations in LES relying on a *shear-improved Smagorinsky model* will be examined in section III.

II. SMOOTHING ALGORITHMS FOR MEAN-FLOW EXTRACTION

Statistical ensemble average may be approximated by space average over directions of homogeneity, whenever it is possible. When it is not, time average may be used instead. Space average is relevant to simple-geometry flows (with directions throughout which fluctuations can be considered as statistically homogeneous), whereas time average is adequate when the flow (its mean and its fluctuations) remain statistically stationary in time. In the presence of deterministic unsteadiness, such as vortex shedding or blade passing in a turbomachine, these two approximations must clearly be abandoned. Therefore, a more general procedure must be designed to extract the mean velocity field and track its possible evolution when large-scale instabilities develop in the flow.

Our proposal is based on weighted moving average in time, which may be viewed as a generic smoothing operation that highlights longer-term variations or cycles but erases rapid fluctuations. It is here assumed that the mean flow is given (at each grid point) by the low-frequency component of the velocity field, and that the turbulent component of the flow adds

itself to this “unsteady mean”. From the viewpoint of signal-processing, extracting a low-frequency trend from a time series is a “dangerous technique” that requires to determine *a priori* a cut-off frequency above which excitations should be ignored. This cut-off frequency is well defined if there exists a clear-cut separation in the power-spectrum of the signal, so that a low-frequency component may be clearly isolated from the high frequencies. Also, it assumes that the separation between the mean-flow and such fluctuations is stationary. In the present context of turbulent flows, there is no clear separation in frequency, as fluid dynamics is known to exhibit large-band spectra [25], and steadiness is not always achieved either. Accordingly, a specific strategy has been elaborated here in order to separate trends from fluctuations in our velocity time series.

Two distinct algorithms are proposed, based on existing well-known smoothing schemes. They are presented in details and discussed in relation to their application to mean-flow extraction. Firstly, we introduce an exponentially-weighted moving average (also called *exponential smoothing*) with a fixed smoothing factor, hence a stationary method. This basic method should be considered as a baseline approach, a starting point for comparisons with more elaborated smoothing methods. Then, an adaptive Kalman filter is presented as a refinement of the exponential smoothing that does not require an *a priori* stated value for the cut-off frequency but only the prescription of an interval relevant for this frequency; the cut-off frequency adapts itself dynamically within this interval according to the recent history of the signal. These two methods are now presented.

A. Exponentially-weighted moving average

A simple proposal for extracting the low-frequency component of the velocity field is a moving (unweighted) arithmetic average of the velocity time signal over an interval of length $\tau_c = (N - 1)\Delta t$, where Δt is the time step and N is the number of points retained in the average. This method corresponds to a low-pass filtering with a cut-off frequency $f_c \sim 1/\tau_c$ that should be identified with some characteristic frequency (stemming from the ratio of a characteristic velocity and a characteristic length in the flow). Unfortunately, this simple technique requires the storage of the last N instants in order to maintain a constant f_c . This appears to be prohibitive in memory when processed at each mesh-point of a three-dimensional grid (with an integration time step typically much smaller than the

cut-off period). Another disadvantage is that it cannot be used on the first $N - 1$ instants.

These limitations are alleviated by an *exponentially-weighted moving average*, also referred to as *exponential smoothing* in the literature and originally introduced in the works of Brown and Holt in the 1950s (see, e.g., the reviews in [10, 11, 14]). The main point is to update at each time step the previous estimate of the mean by taking into account the new data point. Let us denote by $[u]^{(n)}$ the estimated mean of one component of the velocity at time n and at some arbitrary mesh-point. The update of this estimated mean writes in a recurrence form:

$$[u]^{(n+1)} = (1 - c_{\text{exp.}}) [u]^{(n)} + c_{\text{exp.}} u^{(n+1)} \quad (8)$$

with $[u]^{(0)} = u^{(0)}$ at initial time and the smoothing factor $0 < c_{\text{exp.}} < 1$. This algorithm requires only the storage of the mean $[u]$, which is a major improvement over the arithmetic average. The smoothing factor $c_{\text{exp.}}$ somehow controls the range of past iterations influencing the estimation of the mean. From (8), an older data point at instant m contributes to the mean flow at instant $n + 1 > m$ with an exponentially decreasing weight $(1 - c_{\text{exp.}})^{n+1-m} \times c_{\text{exp.}}$, therefore giving more importance to the recent observations while still not discarding older observations entirely.

To be physically sound, $c_{\text{exp.}}$ should be related to the cut-off frequency of this smoothing. In order to exhibit this relation, we shall reformulate (8) under the form of a digital filter [23]. Firstly, let us recall the general z -transform applied to a discrete-time process $X^{(n)}$: $X^{(n)} \rightarrow \widehat{X}(z) = \sum_n X^{(n)} z^{-n}$. The z -transform applied to (8) yields

$$\widehat{[u]}(z) = \frac{c_{\text{exp.}}}{1 - (1 - c_{\text{exp.}})z^{-1}} \widehat{u}(z).$$

By considering $z = e^{i\omega\Delta t}$ (the relation between z and the analog harmonic frequency ω when the signal has sampling period Δt), one gets that the power-spectra of $[u]^{(n)}$ and $u^{(n)}$ are linked by the transform

$$\left| \widehat{[u]}(\omega) \right|^2 = \frac{c_{\text{exp.}}^2}{|e^{i\omega\Delta t} - (1 - c_{\text{exp.}})|^2} \cdot |\widehat{u}(\omega)|^2,$$

which is a discrete-time first-order low-pass filter. The cut-off frequency f_c , at which the amplitude is reduced by half [37], is given by

$$\frac{c_{\text{exp.}}}{|e^{i\omega_c\Delta t} - (1 - c_{\text{exp.}})|} = \frac{1}{2} \quad \text{with} \quad \omega_c = 2\pi f_c.$$

Solving directly this equation gives $c_{\text{exp.}} = \left(\sqrt{6\alpha_c + \alpha_c^2} - \alpha_c \right) / 3$ with $\alpha_c = 1 - \cos(\omega_c\Delta t)$.

In practical LES, $\omega_c \Delta t \ll 1$ (a necessary condition for time integration) and therefore $c_{\text{exp.}} \simeq \omega_c \Delta t / \sqrt{3}$, which finally yields

$$c_{\text{exp.}} \simeq \frac{2\pi f_c \Delta t}{\sqrt{3}} \approx 3.628 f_c \Delta t. \quad (9)$$

This first method acts as a low-pass filtering on the velocity time signal with a fixed cut-off frequency. The main advantage of this method is its simplicity, both conceptually and in its implementation. The computational cost is also very low. However, a known limitation (as already mentioned) is the difficulty to pick an appropriate cut-off frequency for the whole flow. As argued in [10], this parameter is dangerous to be guessed at and is better estimated from the data. Unavoidably, there is a trade-off between the ability to follow faithfully a quick evolution of the mean, which requires a cut-off frequency (and therefore $c_{\text{exp.}}$ not too small), and the capacity to smooth out correctly the fluctuations, for which a small cut-off frequency is usually better. Moreover, for a slowly evolving mean-flow, there is an inevitable delay (induced by the exponential smoother) with respect to the proper dynamic. This delay is given by the *group delay* at null frequency: $\Delta t / c_{\text{exp.}}$ [23], so the smaller $c_{\text{exp.}}$ is, the larger the delay is. These restrictions make difficult the *a priori* estimation of the relevant cut-off frequency when the flow is strongly non-homogeneous and unsteady. A more flexible algorithm is wanted, capable of adapting itself to the local behavior of the flow. This had led us to design a second algorithm based on Kalman filtering.

B. Adaptive Kalman filtering

A more elaborated way to extract the mean velocity field is by use of a Kalman filter [14]. In brief, a Kalman filter is a recursive filter that estimates the state of a dynamic system, here the mean velocity of the flow, from a series of measurements (or observations). Kalman filtering is a major topic in control theory and control systems in engineering science, and is known to be rather efficient [6, 14]. An important feature of this filter is its formulation as a recursive estimator, in which the updated state is computed from the previous state and the current measurement only (as for the exponential smoothing). Moreover, being adaptive in nature, the Kalman filter is expected to allow for a better control and adjustment to the low-frequency behavior of the flow, especially in localized regions where instabilities develop (in the vicinity of an obstacle, for instance). From a computational viewpoint, it is therefore

an interesting alternative solution to the exponential smoothing.

The problem can be formulated quite simply in a *state-space representation*, in which the mean velocity (at each mesh-point) represents the state variable of the system and the instantaneous velocity is an observation:

$$\begin{cases} [u]^{(n)} = [u]^{(n-1)} + \delta[u]^{(n)} \\ u^{(n)} = [u]^{(n)} + \delta u^{(n)}. \end{cases} \quad (10)$$

This is the state-space representation of a random walk model with noise [14], the noise representing here the fluctuations added to the mean-flow. In this form, the mean velocity adjusts itself at each time step with some control increment $\delta[u]^{(n)} = [u]^{(n)} - [u]^{(n-1)}$. The measurement equation expresses the deviation of the instantaneous velocity from the estimated mean: $\delta u^{(n)} = u^{(n)} - [u]^{(n)}$. These two quantities are modeled as random processes with zero mean and normal variance. Here, it is assumed that the evolution of the mean velocity is (very) slow compared to the evolution of the instantaneous velocity, so that no deterministic evolution is prescribed for $[u]$: $[u]^{(n)} = [u]^{(n-1)}$ *a priori*. However, $[u]$ is authorized to evolve (like a sort of biased random walk) if the observation departs significantly from the mean. In our model, the variance of $\delta[u]$ is fixed but the variance of δu is updated dynamically as the simulation evolves. This strategy allows the instantaneous velocity to depart significantly from its mean, which is expected to fluctuate in a more gentle manner.

The preliminary step is the initialization of the algorithm. Initially, the mean is fixed at $[u]^{(0)} = u^{(0)}$. The root mean square of $\delta[u]$ is kept constant throughout the iterations (as previously mentioned) and fixed at

$$\sigma_{\delta[u]} = \frac{2\pi f_c \Delta t}{\sqrt{3}} u^*, \quad (11)$$

where u^* should be interpreted as a “reference velocity” representative of large-scale turbulence (e.g., in a plane-channel flow u^* should be identified with the *friction velocity* at the wall). This essential choice for $\sigma_{\delta[u]}$ stems from the property that, in a steady regime for the mean-flow, our Kalman filter should behave as an exponential smoothing with smoothing factor $c_{\text{exp.}} = \sigma_{\delta[u]}/\sigma_{\delta u}$ (as briefly demonstrated in [38]). Thus, our expression for $\sigma_{\delta[u]}$ is consistent with the requirement that, for stationary periods, $\sigma_{\delta[u]}/\sigma_{\delta u} \simeq 2\pi f_c \Delta t/\sqrt{3}$ (according to (9)) with $\sigma_{\delta u} \simeq u^*$. Finally, the error covariance, which enters in the computation of the optimal Kalman gain (see below), is initialized by $P^{(0)} = \sigma_{\delta u}^2{}^{(0)}$ with $\sigma_{\delta u}^{(0)} = \sigma_{\delta[u]}$.

Standard calculations express a Kalman filter in a recursive form implying two distinct phases: *predict* and *update*. The “predict phase” uses the state estimate from the previous timestep to produce a prediction at the current timestep. In the “update phase”, measurement information at the current timestep is used to refine this prediction by use of an optimal Kalman gain. Accordingly, the complete algorithm (following the standard theory of Kalman filtering [6, 14]) organizes as follows:

Predict:

— the mean estimate does not *a priori* change: $\widetilde{[u]}^{(n+1)} = [u]^{(n)}$. The error covariance is predicted as $\widetilde{P}^{(n+1)} = P^{(n)} + \sigma_{\delta[u]}^2$.

Update:

— the optimal Kalman gain is given by

$$K^{(n+1)} = \widetilde{P}^{(n+1)} \times \frac{1}{\widetilde{P}^{(n+1)} + \sigma_{\delta u}^2} \quad (12)$$

and the updated mean estimate is obtained by the “correction equation”

$$[u]^{(n+1)} = \widetilde{[u]}^{(n+1)} + K^{(n+1)} \times (u^{(n+1)} - \widetilde{[u]}^{(n+1)}). \quad (13)$$

This expression is reminiscent of (8) for the exponential smoothing. Here, the Kalman gain acts as an instantaneous equivalent of the smoothing factor c_{exp} .

— the error covariance is updated (for the next iteration) by

$$P^{(n+1)} = \widetilde{P}^{(n+1)} - K^{(n+1)} \times \widetilde{P}^{(n+1)}.$$

Finally, in order to the Kalman filter adaptive, an estimate of the variance of δu is required. For this purpose, we suggest the following formula

$$\sigma_{\delta u}^2{}^{(n+1)} = \max\left(\widetilde{\sigma}_{\delta u}^2, 0.1 \times u^{*2}\right) \quad (14)$$

$$\text{with } \widetilde{\sigma}_{\delta u}^2 = u^* \times \left| [u]^{(n+1)} - u^{(n+1)} \right|. \quad (15)$$

The estimator (15) is *ad-hoc* and devised to yield a physically-sound estimation of the variance of the fluctuating velocity: u^* is fixed while $|[u]^{(n+1)} - u^{(n+1)}|$ takes into account the observed (instantaneous) fluctuation. The maximum used in (14) prevents $\sigma_{\delta u}^2$ from vanishing because, in that case, the mean estimate would then stick to the instantaneous velocity for all subsequent time steps. Indeed, if $\sigma_{\delta u}^2{}^{(n)} \simeq 0$ then $K^{(n+1)} \simeq 1$ and $[u]^{(n+1)} \simeq$

$u^{(n+1)}$, consequently $\sigma_{\delta u}^2{}^{(n+1)} \simeq 0$, etc. The value $0.1 \times u^{*2}$ acts as a (non-zero) lower bound for $\sigma_{\delta u}^2$. This bound is reached in regions where the flow is laminar and smooth, and permits to track the onset of turbulence when it occurs: when fluctuations grow, the estimated observation variance $\sigma_{\delta u}^2{}^{(n)}$ increases and $K^{(n+1)}$ decreases, etc. The fluctuating part is therefore well separated from the mean flow which has lower frequencies. Generally speaking, one cannot expect to extract a mean component from instantaneous variations without specifying at least a range of time scales potentially relevant for the evolution of the mean component; (14) and (15), and the maximum therein, fulfill this role.

This algorithm has a computational cost that is higher than the simple exponential smoothing. However, it has the advantage of being able to adjust itself dynamically to unsteadiness of the mean flow and the fluctuations. It also makes easier and automatic the prescription of different separation rules from one mesh-point to another in case of strongly non-homogeneous flows.

III. TEST CASES

The previous smoothing algorithms have been implemented in practical LES to estimate the mean velocity field required in the computation of the SGS eddy-viscosity of the *shear-improved Smagorinsky model* [16].

A. The shear-improved Smagorinsky model

The physical arguments developed in the first section about non-homogeneous flows may be formulated analytically, quite straightforwardly, by assuming that the shear is uniform (at least locally). By explicating the scale-by-scale energy budget of *shear turbulence* from the Navier-Stokes equations, L ev eque *et al.* [16] have shown evidence that the SGS eddy-viscosity should encompass two types of interactions: (i) between the mean velocity gradient and the resolved fluctuating velocities (the rapid part of the SGS fluctuations [29]) and (ii) among the resolved fluctuating velocities themselves (the slow part of the SGS fluctuations). The rapid part is related to the large-scale distortion, while the slow part is associated with the Kolmogorov's energy cascade. Interestingly, these developments end up with a *shear-improved Smagorinsky model* (SISM) for the SGS eddy-viscosity, in which it appears that

the shear should be subtracted from the norm of the resolved rate-of-strain tensor:

$$\mu_{\text{sgs}} = \bar{\rho}(C_s\Delta)^2 \left(|\tilde{S}| - |\langle \tilde{S} \rangle| \right), \quad (16)$$

where $C_s \simeq 0.2$ is the standard Smagorinsky constant for homogeneous turbulence, Δ is the grid spacing (computed as the cubic root of the cell volume) and $|\tilde{S}| \equiv \sqrt{2\tilde{S}_{ij}\tilde{S}_{ij}}$ is the norm of the resolved rate-of-strain. This improvement accounts for the large-scale distortion in regions of strong shear (e.g., near a solid boundary) and, at the same time, allows us to recover the standard Smagorinsky model [30] in regions of locally homogeneous and isotropic turbulence (at grid scale). Interestingly, the SISM does not call for any adjustable parameter nor *ad hoc* damping function; it does not use any kind of dynamic adjustment either. First results concerning a plane-channel flow [16] and a backward-facing step flow [33] have shown the good predictive capacity of this model, essentially equivalent to the *dynamic Smagorinsky model* [12], but with a computational cost and a manageability comparable to the original Smagorinsky model.

It is now our motivation to examine how the SISM behaves when implemented in engineering-flow solvers that use coarser grid, relies on lower-order discretization schemes, and are dedicated to complex-geometry unsteady turbulent flows. For this purpose, the previous smoothing algorithms are devoted tools to estimate the average rate-of-strain, $\langle \tilde{S} \rangle$, entering in the SGS eddy-viscosity (16). In practice, computations have been carried out with the solver *Turb'Flow*. The dynamical equations have been presented in section I. Spatial discretization is based on finite volumes for multiblock structured grids. Convective fluxes are interpolated with a four-point centered scheme (4th-order on cartesian grid) and diffusive fluxes with a two-point centered scheme (2nd-order). Time stepping relies on a five-step Runge-Kutta scheme. More details about the *Turb'Flow* solver may be found in [4]. Two test flows are considered. Firstly, a plane-channel flow configuration [27] that allows us to isolate the basic features of wall-bounded flows. Secondly, the flow past a cylinder in subcritical turbulent regime is addressed in order to deal with phenomena such as boundary-layer separation, transition, vortex shedding and its interaction with turbulence.

B. Plane-channel flow

1. Numerical simulation settings

The temporal development of a bi-periodic plane-channel flow is considered from an initially perturbed laminar flow (Poiseuille’s parabolic velocity profile plus a 2% random relative perturbation). In the fully developed turbulent regime, the expected Reynolds number based on the *friction velocity* (at the wall) is $Re_w = \delta \times u_w / \nu = 395$, where δ is the half-width of the channel. The comprehensive direct numerical simulation (DNS) database obtained by Moser *et al.* [19] is used as a reference in the turbulent regime. An illustration of this test case is given in Fig. 1.

The mean flow is oriented along the x -direction and plane walls bound the flow at $y = \pm\delta$ with $\delta = 0.01\text{m}$. Periodicity is imposed in the streamwise and spanwise directions. The computational domain extends over $L_x \times L_y \times L_z = 2\pi\delta \times 2\delta \times \pi\delta$ (same as reference DNS). The grid is cartesian with $49 \times 89 \times 41$ points; a *tanh distribution* is used in the y -direction. In the turbulent regime, the grid spacing is $\Delta x^+ = 52$ (in wall units), $\Delta y^+ = 0.5$ at the wall (11 points below $y^+ = 10$), $\Delta y^+ = 24$ at centerline and $\Delta z^+ = 31$. The pressure is reduced to obtain a Mach number $Ma \simeq 0.2$ at the centerline (in order to optimize the convergence of the compressible solver). The momentum in the x -direction is maintained by a source term that is adjusted dynamically to match the objective centerline mean velocity on the one hand, the friction velocity u_w is a result of the simulation on the other. The numerical results are non-dimensionalized with the characteristic length, δ , and the objective friction velocity, u_w , in order to draw comparisons between the different computations. Finally, three computations have been carried out with the *shear-improved Smagorinsky model* using three distinct smoothing methods:

- *spatial averaging* over x and z directions.
- *exponential smoothing* with a constant smoothing factor c_{exp} over the whole domain. The cut-off frequency is fixed at $f_c = u_w / \delta$ (based on objective u_w), which yields $c_{exp} = 1.07 \times 10^{-4}$ from (9). This cut-off frequency is expected to be representative of the largest eddies and provide a reasonable estimate of the lower bound of the turbulent spectrum.

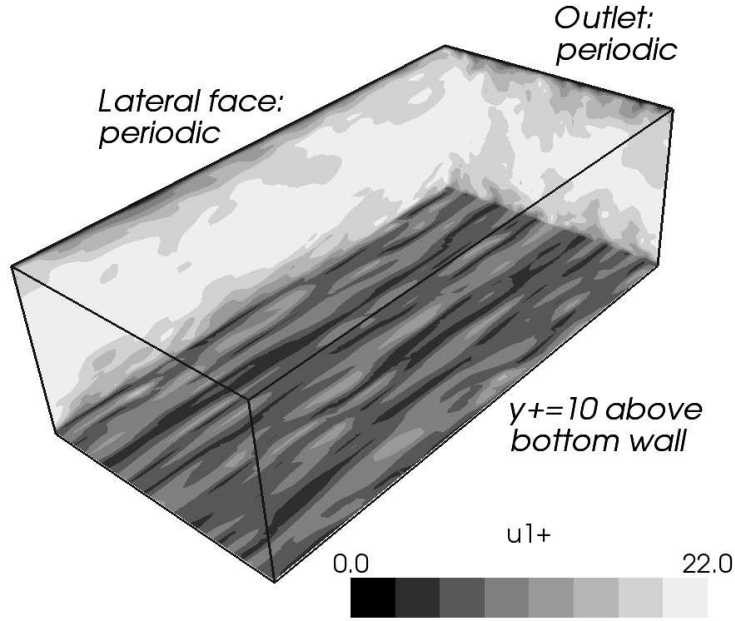


FIG. 1: Instantaneous isocountours of u_1^+ in the turbulent regime (the exponential smoothing is used in the computation of the SGS eddy-viscosity). As expected, the flow becomes turbulent and develops streaky structures in the near-wall region.

— *adaptive Kalman filtering*. In a consistent way with the exponential smoothing,

$$\sigma_{\delta[u]} = \frac{2\pi f_c \Delta t}{\sqrt{3}} u^*$$

with the characteristic velocity $u^* = u_w$ and the cut-off frequency $f_c = u_w/\delta$, where u_w is fixed to its objective value.

2. Instantaneous velocity probes and smoothing methods

The instantaneous velocity component, u_1^+ , probed at location $y^+ = 10$ ($x = 0.19 \times L_x$ and $z = 0.23 \times L_z$) for the three computations is displayed in Fig.2, together with the mean estimate, $[u_1^+]$, resulting from the smoothing algorithms. A transition to turbulence accompanied with the development of turbulent fluctuations and the increase of the mean velocity is observed for $6 \leq t^+ \leq 12$. Regarding the smoothing operations, the high frequencies are obviously suppressed. However, some low-frequencies persist in the cases of the exponential smoothing and the Kalman filtering, as expected from their low-pass behavior. The spatial average (Fig.2(a)) suppresses nearly all the fluctuations in the turbulent regime and cap-

tures the evolution of the mean velocity from the laminar to the turbulent regime. It is very efficient, however, it requires spatial homogeneity of the flow in x and z directions, which is hardly met in more complex configurations.

The cut-off period of the exponential smoothing (Fig.2(b)) was fixed at $T_c^+ = 1$. Fluctuations of the velocity exceeding this period are therefore maintained. Besides, the characteristic time related to advection through the whole channel may be estimated as $\Delta t_{conv.}^+ = L_x^+ / \langle u_1^+ \rangle \simeq 0.48$ at $y^+ = 10$. Consequently, the exponential smoothing retains fluid structures whose period is larger than $\Delta t_{conv.}^+$. Such dynamical events may be artificially trapped between the periodic boundaries, passing several times in circles through the channel and thus enforcing temporal correlation and weakening the smoothing. This streamwise periodicity is an artifact of the channel-flow configuration that should not occur in practical configurations; the exponential average should then be more regular.

For comparison, the spatial average in the x -direction is calculated *a posteriori*. Interestingly, the x -average follows quite accurately (with a short delay) the variations of the exponential average. This may be explained by the fact that, roughly speaking, the whole velocity profile (along the x -direction) passes through the probe during a time interval $\Delta t_{conv.}^+$ of the order of the “memory time”, T_c^+ , of the exponential smoothing. Therefore, the exponential average (in time) is mainly equivalent to the spatial average (in the streamwise direction). However, this former does not require any homogeneity conditions, it is local in space and time whereas the x -average uses here a 48-point stencil. Finally, the adaptive Kalman filtering (Fig.2(c)) behaves qualitatively in a similar way as the exponential smoothing but with a cut-off frequency that adapts itself locally. Here, at $y^+ = 10$, this seems to give smoother results. This feature will be investigated next.

3. Mean velocity profiles and energy spectra

The mean velocity profile and the turbulent intensity profiles (in the stabilized turbulent regime) are displayed in Fig.3 and compared with DNS data. In the post-processing, the average (denoted by $\langle \rangle$) is meant over space (x and z directions, y -mirror) and time (111 samples for $11.8 \leq t^+ \leq 28.0$). A good prediction of the mean velocity profile is achieved over the different sublayers. The choice of the smoothing method (used to compute the SGS eddy-viscosity) does not affect significantly the results. The resulting friction velocity u_w is

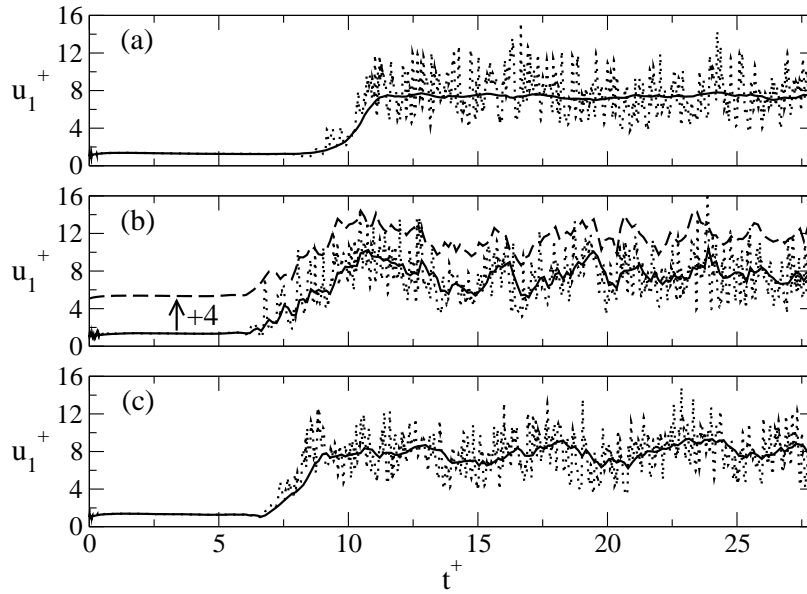


FIG. 2: Numerical velocity probes at $y^+ = 10$ ($x = 0.19 \times L_x$ and $z = 0.23 \times L_z$) for LES using spatial average (a), exponential smoothing (b) and adaptive Kalman filtering (c) to evaluate the mean velocity field as the simulation is running. Dots: instantaneous velocity, u_1^+ . Continuous lines: estimated mean velocity, $[u_1^+]$. The dashed-line in (b) is the post-processed spatial average over the x -direction; the plot has been shifted vertically (+4) for clarity.

0.53m/s for spatial averaging and 0.54m/s for the exponential smoothing and the adaptive Kalman filtering. This is 10% below the objective value $u_w = 0.59\text{m/s}$ (from the DNS) but within the level of accuracy reviewed by [28] for standard SGS models. Fluctuating velocities are also well captured, considering the levels and evolutions for the three components, and no significant difference is observed between the computations.

The spanwise spectra of the axial velocity are shown in Fig.4 for wall-normal distances $y^+ = 10$ and $y^+ = 100$. Again, the three smoothing methods lead to very similar results. The LES spectra are in close agreement with the DNS spectra in the range of energy-carrying wavenumbers and the dependence on y^+ is suitably captured.

4. Two-point velocity auto-correlations

The two-point velocity autocorrelations in the streamwise and spanwise directions are displayed in Fig.5 for $y^+ = 10$ and $y^+ = 100$. Interestingly, our LES appear particularly effective in capturing the correct dependence on the separation distance. Again, the choice

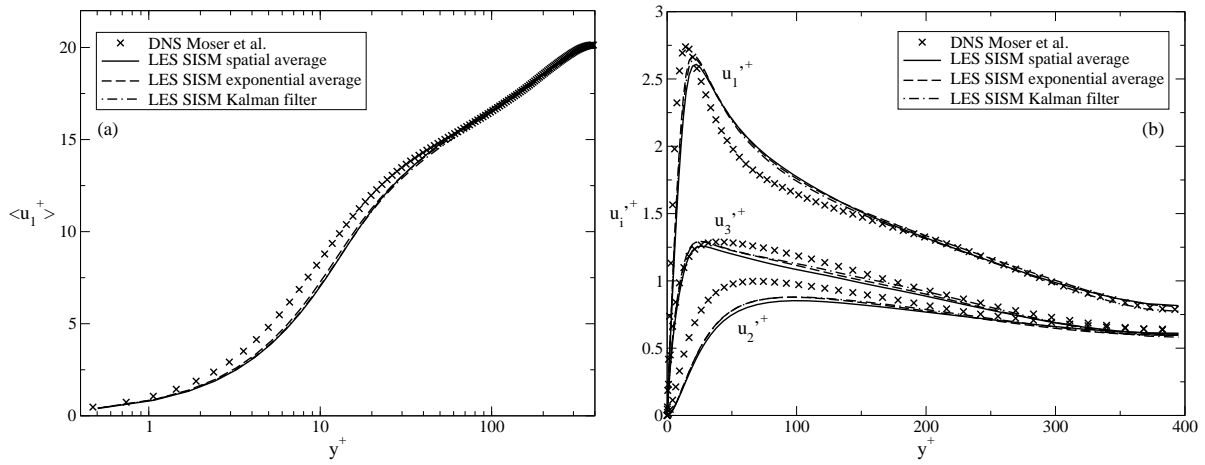


FIG. 3: Mean axial velocity profile (a) and turbulent intensity profiles (b).

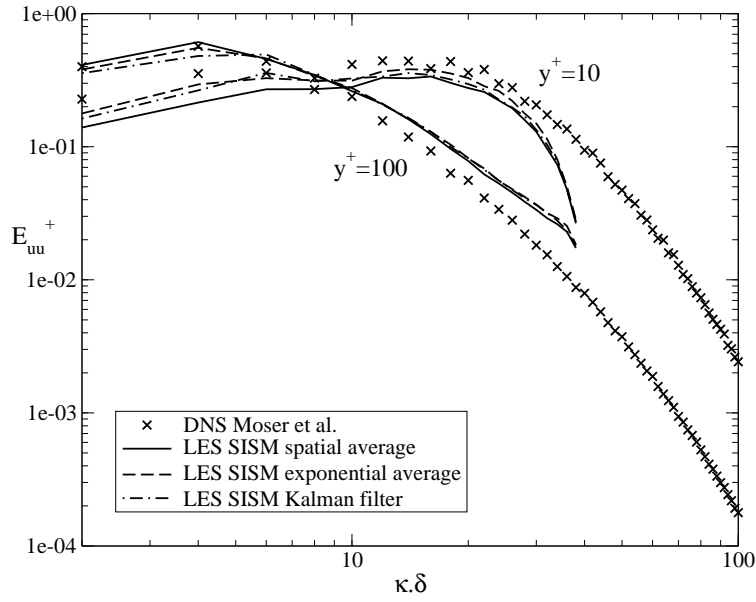


FIG. 4: Spanwise spectra of the axial velocity.

of the smoothing method has no noticeable effect on these two-point quantities. The major trends are fulfilled, that is to say, (i) the correlations spread further in the direction of the flow (x -direction) because of the streaky structures (evidenced in Fig.1) and (ii) when y increases, correlations spread (in x and z directions) and anisotropy is reduced between the velocity components. Let us remark also that the periodic boundary conditions and the domain extent do not allow for a proper decorrelation in x -direction, as shown particularly by R_{11} at $y^+ = 100$.

Finally, the correlation times of the three components of the fluctuating velocity, given

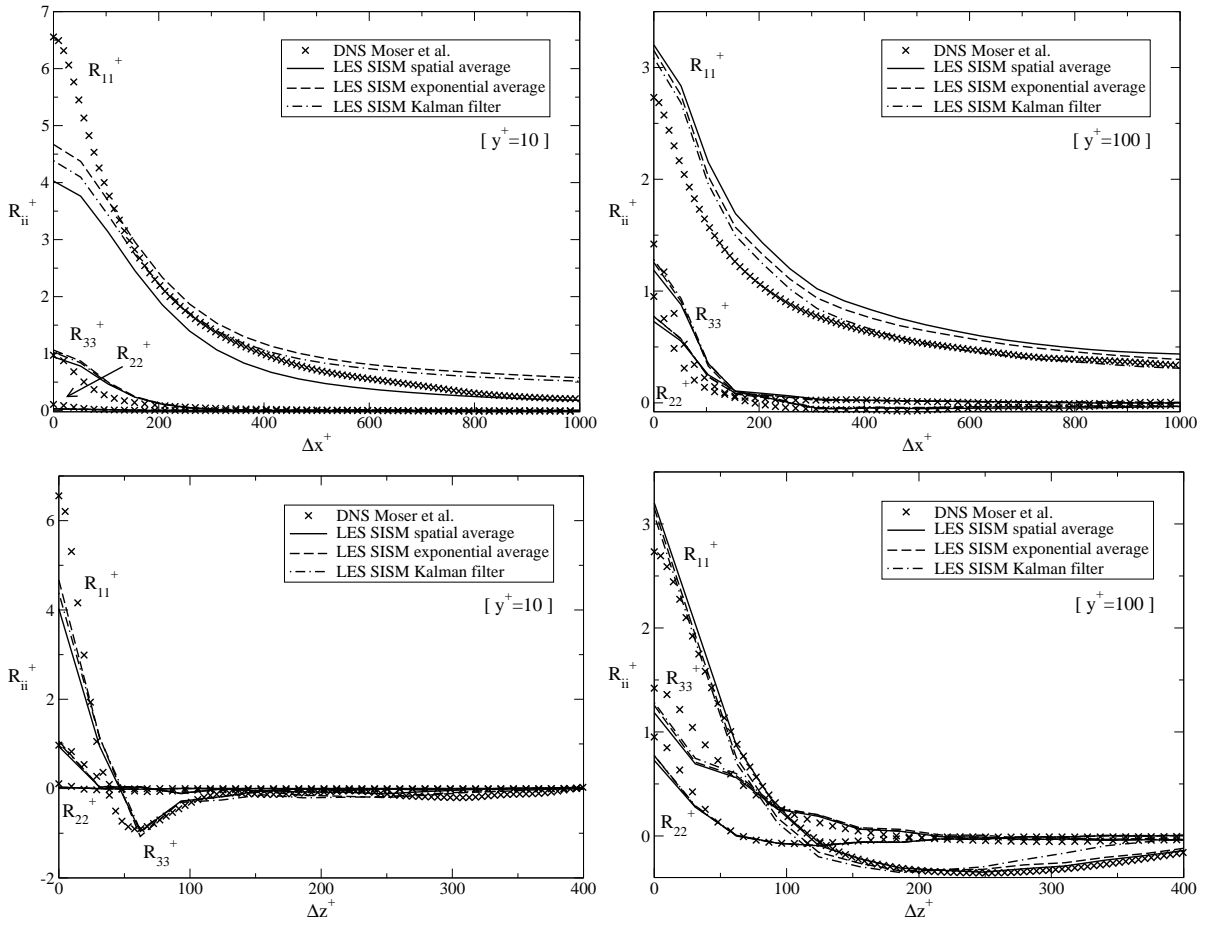


FIG. 5: Two-point velocity auto-correlations for streamwise separations (up) and spanwise separations (down) at $y^+ = 10$ (left) and $y^+ = 100$ (right).

respectively by $\langle u'_i(t)u'_i(t + \tau_{ii}) \rangle = 1/2$ for $i = 1, 2, 3$, are plotted in Fig. 6. Here, average is meant over space (z direction and y -mirror) and time (3000 samples for $28.6 \leq t^+ \leq 29.5$). Only the results for the exponential smoothing are reported. It is found that the correlation times globally decreases with the distance from the wall, and that τ_{11} dominates over τ_{22} and τ_{33} . The cut-off period of the exponential smoothing ($T_c^+ = 1$) and the mean cut-off period of the Kalman filter are also displayed in the figure. This latter is obtained by identifying the optimal Kalman gain (K) with the smoothing factor of an exponential smoothing and by using (9) in order to relate this smoothing factor to $T_c \equiv 1/f_c$. This finally yields $T_c^+ = 2\pi\Delta t^+ / \sqrt{3}K$. The two cut-off periods are found about 20 times larger than the correlation times of the velocity fluctuations, indicating that the two smoothing methods are indeed efficient at filtering out turbulent fluctuations. The mean cut-off period of the Kalman filter remains close to 1 but decreases with the wall-normal distance, following

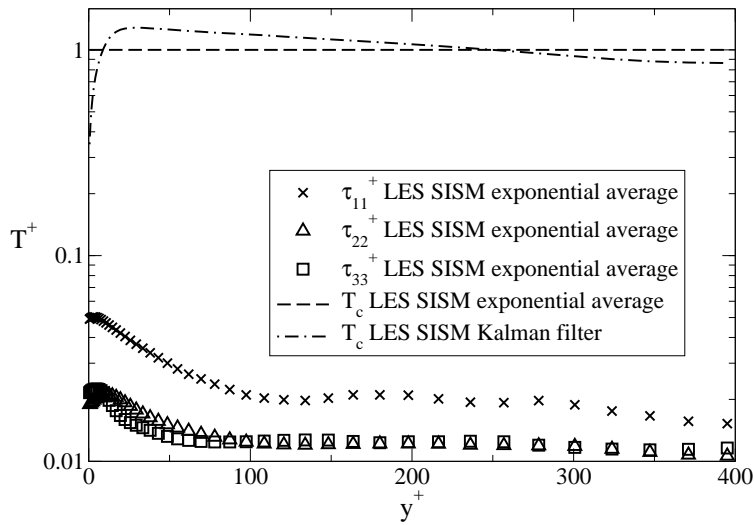


FIG. 6: Correlation times of the three components of the fluctuating velocity and cut-off periods, T_c^+ , of the exponential smoothing and adaptive Kalman filtering.

the behavior of the velocity correlation times. This is very reasonable since the Kalman filter is expected to adapt its cut-off period according to the observed velocity fluctuations. However, in this test case the spatial variation of the correlation times is rather moderate, which explains that the cut-off period of the adaptive Kalman filter remains actually very close to the constant cut-off period of the exponential smoothing. The two methods behave therefore mostly the same way.

In summary, our LES results for the channel flow are in very good agreement with reference DNS data for both one-point and two-point statistics. Regarding the SISIM, the exponential smoothing and the adaptive Kalman filtering achieve very comparable results.

C. Flow past a cylinder in the subcritical turbulent regime

A major advantage of the exponential smoothing and adaptive Kalman filtering is that they do not *a priori* require spatial homogeneity nor steadiness (of the mean flow). In this section, the flow past a circular cylinder in the subcritical turbulent regime is investigated and the focus is on the exponential smoothing. The idea is here to test how a *basic* smoothing method can behave in a more severe test case (the study of the adaptive Kalman filter in this flow configuration is postponed to a future work). As highlighted in [26], the numerical simulation of flows past bluff bodies is a great challenge for LES. One of these more chal-

lenging test case is the flow past of a circular cylinder at high Reynolds number [5]. This is a realistic well-documented test case in the perspective of practical engineering-flow LES.

1. Numerical simulation settings

A circular cylinder of axis z with diameter $D = 0.01$ m is placed in an undisturbed airflow of velocity $U_\infty = 70$ m.s⁻¹ along the x -direction (under standard conditions of temperature and pressure). The diameter-based Reynolds number is $Re_D = 4.7 \times 10^4$ belonging to the subcritical turbulent regime. This flow is complex and experiences laminar boundary layer separation, shear-layer transition in the vicinity of the cylinder, turbulent wake and von Kármán vortex shedding at Strouhal number $St = f_s D / U_\infty \simeq 0.2$, where f_s is the vortex-shedding frequency.

The aspect ratio of the cylinder (span length over radius) has some influence on the flow [31], which explains partly the dispersion of the experimental results. In the simulation, the grid extends over $3D$ in the spanwise direction (z -direction) but periodicity is imposed on the end-planes so that the computation can be representative of higher aspect ratios. In the radial direction, the computational domain extends over $10D$ and the whole mesh uses 3×10^6 points. In the turbulent region after separation, the grid density is $\Delta r_{max}^+ \lesssim 1$, $R\Delta\theta_{max}^+ \lesssim 20$ and $\Delta z_{max}^+ \lesssim 25$ (in wall units). This mesh density respects standard recommendations for LES [27].

The computation uses a fixed smoothing factor $c_{exp} = 6.093 \times 10^{-4}$ over the whole domain. This value of c_{exp} has been obtained from (9) with a cut-off frequency: $f_c = 2f_s$, where $f_s = 1400$ Hz is the expected vortex-shedding frequency (mentioned above). The cut-off frequency of the exponential smoothing is taken above the vortex-shedding frequency to ensure that the large eddies that detach from the cylinder (vortex shedding) are suitably captured in the mean-flow reconstruction.

2. Flow field, characteristic forces and Strouhal number

The mean streamwise velocity is displayed in the upper half of Fig. 7. The grey square dot delimits the recirculation bubble and defines the “wake-closure length” l_c given by $\langle U \rangle(x = l_c, y = 0) = 0$. In the lower half of the figure, the mean-velocity vector field is

displayed and a mean recirculation zone can be clearly identified. In Fig. 8, the instantaneous vorticity (along the z -direction) and the mean-flow vorticity (obtained from the exponential smoothing) are compared at the same instant. While the instantaneous vorticity exhibits a wide range of structure sizes, the exponential-smoothed flow mostly captures the vortex shedding (where shear effects are significant), as expected.

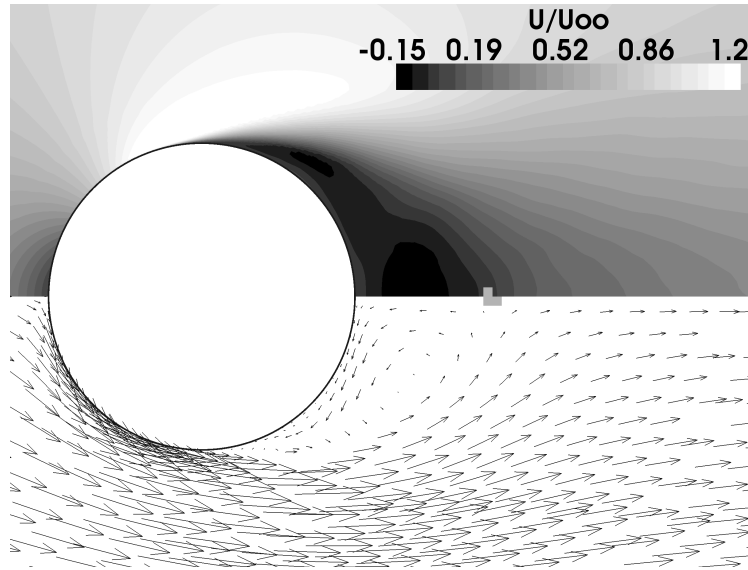


FIG. 7: Mean velocity field (U_p : colormap of the non-dimensionnal streamwise velocity. *Down*: velocity vectors.). The grey square indicates the end of the recirculation bubble.

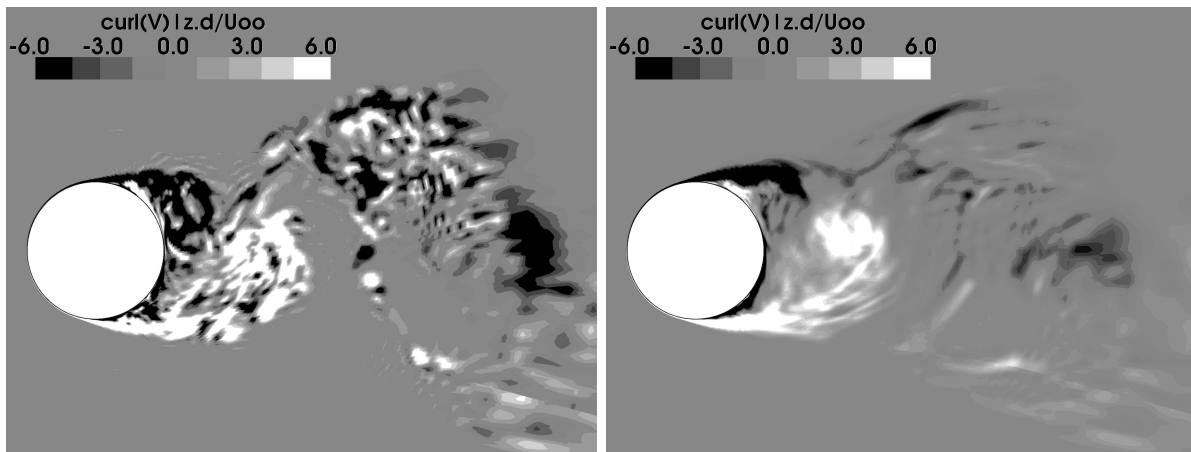


FIG. 8: Non-dimensionnal vorticity field (*left*: instantaneous field; *right*: exponentially-smoothed field at the same instant).

Fig. 9 displays the temporal evolution of the lift coefficient, C_L , and drag coefficient,

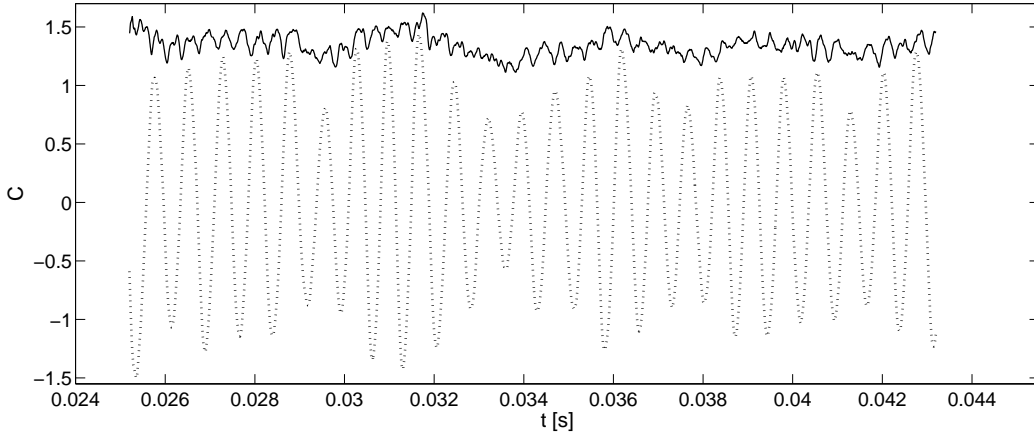


FIG. 9: Temporal evolution of lift and drag coefficients. ...: C_L ; —: C_D .

C_D , over 24 periods of the vortex shedding. As already mentioned in [20, 35], a strong correlation between the variations of C_D and the modulation of C_L is observed. Typically, the value of the drag is high when the lift amplitude is maximum. The time-averaged value of the drag coefficient, $\overline{C_D}$, the root-mean-square drag coefficient, C'_D , and the root-mean-square lift coefficient, C'_L , are gathered in Table I and compared with the results of various experiments. Our numerical results are in good agreement with experimental data, however, lying often in the upper part of confidence ranges.

The vortex-shedding has a strong impact on the pressure field around the cylinder and therefore on the lift and drag oscillations. Except from the rearmost part of the cylinder, the pressure spectrum (in frequency) is peaked around the shedding frequency, f_s . From the wall pressure spectrum at $\theta = 90^\circ$ (θ is the angle taken from the upstream stagnation point), the vortex-shedding frequency has been identified and measured at the value $f_s = 1330Hz$, which corresponds to the Strouhal number $St = 0.19$. In Table I, this key criterion is shown to be in very good agreement with various experimental results.

3. Wall friction and pressure distribution

Fig. 10 shows the distribution of the mean-friction coefficient, $\overline{C_f} \equiv [\overline{\tau_w}/\frac{1}{2}\rho U_\infty^2]\sqrt{Re_D}$, around the cylinder. The mean separation angle, θ_s , is the angle for which $\overline{C_f}$ vanishes. In the present LES, the measured value is $\theta_s = 88.0^\circ$ (with an angular resolution $\Delta\theta = 2^\circ$ in this region). According to experimental data in the range $4.0 \cdot 10^4 \leq Re_D \leq 4.5 \cdot 10^4$ [35], the

	LES	data in litterature
\overline{C}_D : mean drag coefficient	1.34	1.35 [31] ($Re_D = 4.3 \cdot 10^4$) [1.0, 1.35] [7] ($Re_D = 4.8 \cdot 10^4$) [1.0, 1.3] [1] ($Re_D = 4.8 \cdot 10^4$) [1.1, 1.3] [35] ($Re_D \in [10^4, 10^5]$)
C'_D : rms drag coefficient	0.09	0.16 [31] ($Re_D = 4.3 \cdot 10^4$) [0.08, 0.1] [13] ($Re_D = 4.8 \cdot 10^4$) [0.05, 0.1] [35] ($Re_D \in [10^4, 10^5]$)
C'_L : rms lift coefficient	0.77	[0.45, 0.55] [31] ($Re_D = 4.3 \cdot 10^4$) [0.4, 0.8] [13] ($Re_D = 4.8 \cdot 10^4$) [0.6, 0.82] [35] ($Re_D \in [10^4, 10^5]$)
St : Strouhal number	0.19	[0.18, 0.2] [7] ($Re_D = 4.8 \cdot 10^4$) [0.185, 0.195] [22] ($Re_D = 6.1 \cdot 10^4$)

TABLE I: Force coefficients and Strouhal number in comparison with experimental data.

expected separation angle is $\theta_s \approx 83^\circ$. Our result appears therefore slightly over-estimated, however, the discrepancy is only two grid points.

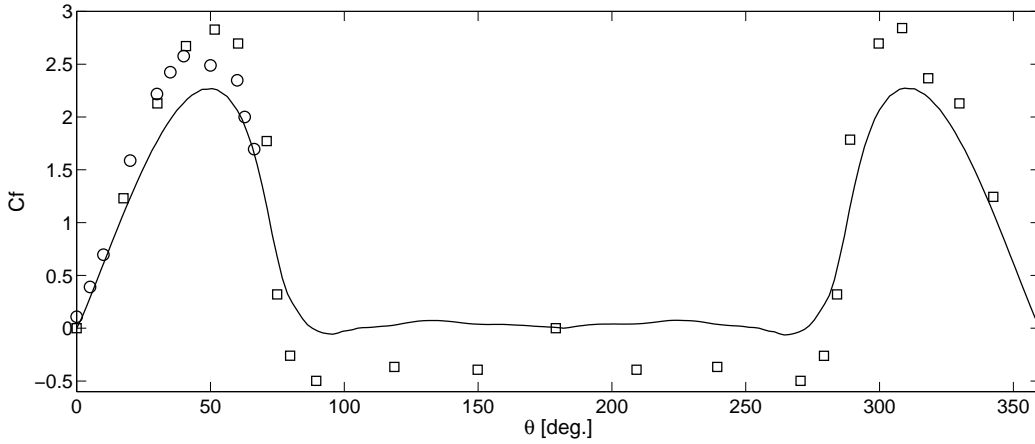


FIG. 10: Circular cylinder skin friction. —: simulation at $Re_D = 4.7 \times 10^4$; \circ : exp. data at $Re_D = 9.1 \times 10^4$ [34]; \square : exp. data at $Re_D = 10^5$ [1].

In the channel-flow test case, the cut-off frequency has been evaluated by $f_c = u_w/\delta$ with δ being the half width of the channel (reference length of the flow) and u_w the friction

velocity (reference velocity based on the shear at the wall). Along the same line, a cut-off frequency may be devised here from the radius of the cylinder ($R = D/2$) and the maximal value of skin friction velocity on the cylinder, that is

$$f = \frac{\max(u_w)}{R}. \quad (17)$$

This frequency, representative of the largest turbulent eddies, yields $f = 1430$ Hz. Interestingly, this is almost equal to the vortex-shedding frequency ($f_s = 1400$), which characterizes the mean flow unsteadiness. Consequently, in this test-case, positioning the cut-off at $f_c = 2 \times f_s$ allows the expected separation of the mean and turbulent fluctuations (the factor 2 is arbitrary). Only the low-frequency end of the turbulent spectrum is included within the mean component.

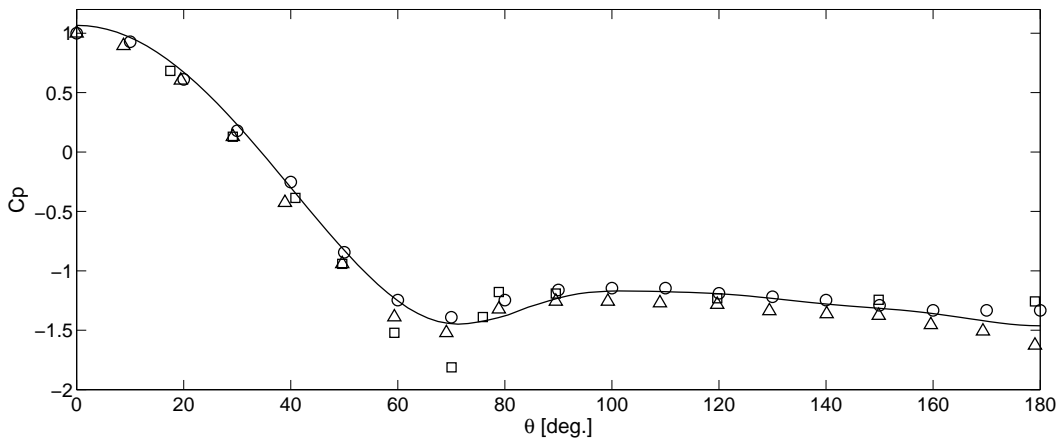


FIG. 11: Mean pressure-coefficient distribution, \overline{C}_p , around the cylinder. —: simulation at $Re_D = 4.7 \times 10^4$; \triangle : exp. data at $Re_D = 4.0 \times 10^4$ [31]; \circ : exp. data at $Re_D = 4.6 \times 10^4$ [2]; \square : exp. data at $Re_D = 10^5$ [1].

The distribution of the mean pressure coefficient, $\overline{C}_p \equiv (\overline{p} - p_\infty)/\frac{1}{2}\rho U_\infty^2$, around the cylinder is shown in Fig. 11 and compared with various experimental data. The agreement is very satisfactory. Finally, the distribution of the root-mean-square pressure coefficient, C'_p , is plotted in Fig. 12. The overall behaviour is well-captured, with a maximum around the point of separation [34], but the intensity is over-estimated by approximately 40%. However, the data reported in the figure show a dependence on the Reynolds number which may explain, to some extent, the observed discrepancy.

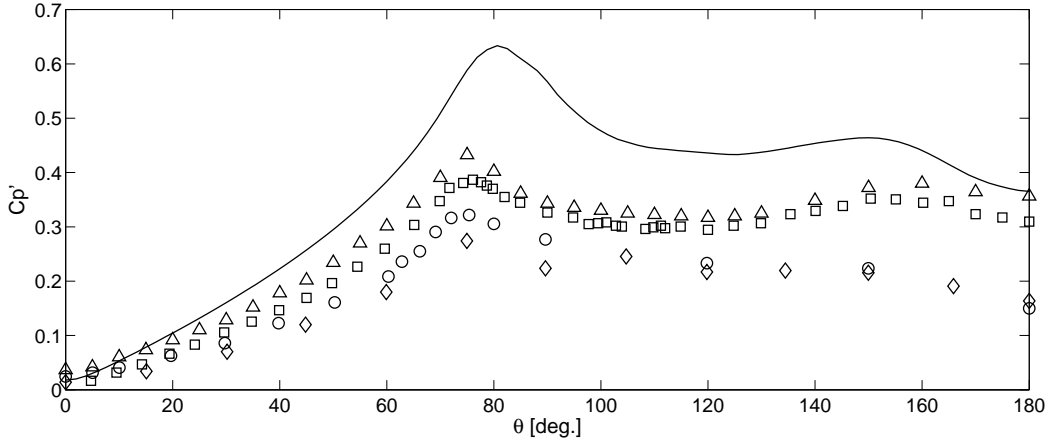


FIG. 12: Root-mean-square pressure-coefficient, C'_p , around the cylinder. —: simulation at $Re_D = 4.7 \times 10^4$; \square : exp. data at $Re_D = 6.1 \times 10^4$ [22]; \triangle : exp. data at $Re_D = 6.1 \times 10^4$ [20]; \circ : exp. data at $Re_D = 10^5$ [34]; \diamond : exp. data at $Re_D = 10^5$ [3].

4. Wake-centerline mean velocity

Fig. 13 shows the mean velocity along the wake centerline. The mean separation bubble length (or wake closure length) is found very close to the cylinder diameter: $l_c \simeq D$. This result is rather low compared to the expected value of $l_c \simeq 1.25 D$ observed in various experiments [21]. Surprisingly, the present results are found closer to the experimental results reported in [7] at $Re_D = 1.4 \times 10^5$.

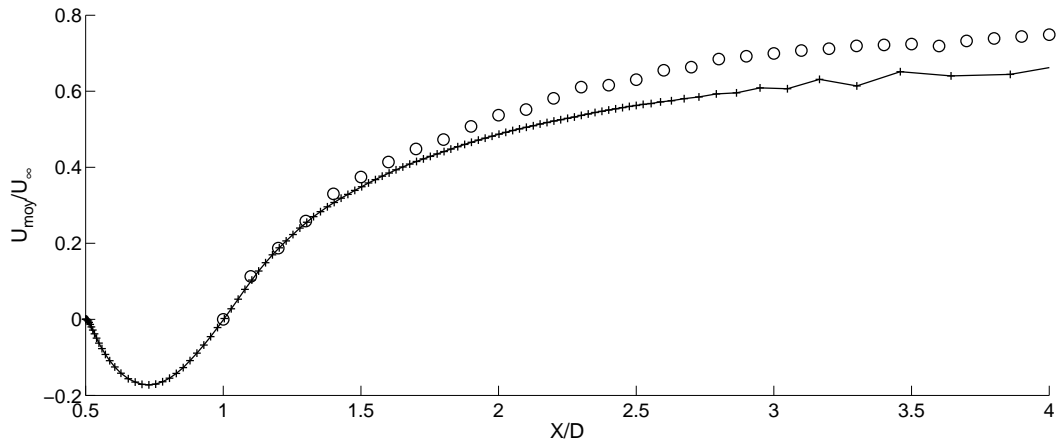


FIG. 13: Mean velocity along the wake centerline. —: simulation with $Re_D = 4.7 \times 10^4$; \circ : exp. data at $Re = 1.4 \times 10^5$ [7].

In summary, the LES of the flow past a cylinder at $Re_D = 4.7 \times 10^4$ relying on the SISM with the use of the exponential smoothing was found to be in very good agreement with the experimental data, concerning the mean and fluctuating values of the aerodynamic forces, the vortex shedding frequency (through the Strouhal number) and the mean distributions of pressure and friction around the cylinder. The mean separation angle, the mean recirculation bubble length and the distribution of the root-mean-square pressure coefficient exhibited some discrepancies, but in an acceptable range.

IV. SUMMARY AND CONCLUSION

From a physical viewpoint, the idea which underlies this study is to take into account the mean-flow inhomogeneities in the estimate of the SGS eddy-viscosity. This is clearly encompassed in the *shear-improved Smagorinsky model*. From a numerical viewpoint, two smoothing algorithms are proposed as workable tools devised to extract the mean velocity field as the LES progresses. Our results indicate that the whole modeling offers an equitable compromise between the accuracy of the numerical solution and the corresponding computational cost. Since the method exploits the temporal discretization recurrently, it is entirely local in space, and therefore, suitable for parallelization and convenient for boundary conditions. Another major advantage is that it does not call for any ad-hoc parameters; all parameters are physically-sound and may be fixed by simple arguments.

In the classical channel flow test-case, this approach was shown to give good results, regarding mean and fluctuating velocities, spectra and two-point correlations. The sub-critical turbulent flow past a cylinder has provided a more selective test-case, combining non-homogeneity and mean-flow unsteadiness, for which the present methods are designed. The basic exponential smoothing gave good results on this configuration, known as particularly challenging. The mean forces, Strouhal number, wall pressure and friction are in very good agreement with various experimental data, and discrepancies on fluctuating wall pressure and wake-centerline mean velocity are limited. Applications to proper turbomachine flows are now investigated.

Acknowledgements:

The authors would like to thank J.-P. Bertoglio, P. Flandrin, L. Shao and F. Toschi for long-term valuable discussions. Numerical simulations rely on the Turb'Flow solver, originating from the LMFA at the Ecole centrale de Lyon and co-developed with the FLUOREM company (France). Simulations have been performed by using the local computing facilities at LMFA and ENS-Lyon (PSMN).

- [1] E. Achenbach. Distribution of local pressure and skin friction around a circular cylinder in cross-flow up to $Re = 5 \times 10^6$. *J.Fluid Mech.*, 34:625–639, 1968.
- [2] E. A. Anderson and A. A. Szewczyk. Effects of a splitter plate on the near wake of a circular cylinder in 2 and 3-dimensional flow configurations. *Experiments in Fluids*, 23:161–174, 1997.
- [3] J. P. Batham. Pressure distributions on circular cylinders at critical reynolds numbers. *J.Fluid Mech.*, 57:209–228, 1973.
- [4] J. Boudet, J. Caro, L. Shao, and E. L ev eque. Numerical studies towards practical large-eddy simulation. *Journal of Thermal Science*, 16(4):328–336, 2007.
- [5] Michael Breuer. A challenging test case for large eddy simulation: high reynolds number circular cylinder flow. *Journal of Heat and Fluid Flow*, 21:648–654, 2000.
- [6] P. J. Brockwell and R. A. Davies. *Time series : theory and methods (Second Edition)*. Springer series in statistics, 1991.
- [7] B. Cantwell and D. Coles. An experimental study if entrainment and transport in the turbulent near wake of a circular cylinder. *J.Fluid Mech.*, 136:321–374, 1983.
- [8] J.-P. Chollet and M. Lesieur. Parametrization of small scales of three-dimensional isotropic turbulence utilizing spectral closures. *Journal Atmospheric Sciences*, 38:2747, 1981.
- [9] U. Frisch. *Turbulence: The Legacy of A. N. Kolmogorov*. Cambridge University Press, 1995.
- [10] E. Gardner. Exponential smoothing: The state of the art. *Journal of Forecasting*, 4:1–48, 1985.
- [11] Everette Jr. Gardner. Exponential smoothing: The state of the art–part ii. *International Journal of Forecasting*, 22(4):637–666, 2006.
- [12] M. Germano, U. Piomelli, P. Moin, and W. H. Cabot. A dynamic subgrid-scale eddy-viscosity

model. *Phys. Fluids A*, 3:1760, 1991.

- [13] J. H. Gerrard. An experimental investigation of the oscillating lift and drag of a circular cylinder shedding turbulent vortices. *J.Fluid Mech.*, 11:244–256, 1961.
- [14] A. Harvey. *Forecasting, Structural series model and the Kalman filter*. Cambridge University Press, 1989.
- [15] M. Lesieur, O. Métais, and P. Comte. *Large-Eddy Simulations of Turbulence*. Cambridge University Press, Cambridge (UK), 2005.
- [16] E. Lévêque, F. Toschi, L. Shao, and J.-P. Bertoglio. Shear-improved smagorinsky model for large-eddy simulation of wall-bounded turbulent flows. *Journal of Fluid Mechanics*, 570: 491–502, 2007.
- [17] T. S. Lund. On the use of discrete filters for large eddy simulation. In *Proceedings of the Summer Program 1997, Center of Turbulent Research*, pages 83–95, 1997.
- [18] C. Meneveau and J. Katz. Scale-invariance and turbulence models for large-eddy simulation. *Annu. Rev. Fluid Mech.*, 32:1–32, 2000.
- [19] R. D. Moser, J. Kim, and N. N. Mansour. Direct numerical simulation of turbulent channel flow up to $re_\tau = 590$. *Physics of Fluids*, 11(4):943–945, 1999. Brief Communications.
- [20] H. Nishimura and Y. Taniike. Aerodynamic characteristics of fluctuating forces on a circular cylinder. *J. Wind Eng. Ind. Aerodyn.*, 89:713–723, 2001.
- [21] C. Norberg. Ldv-measurements in the near wake of a circular cylinder. *Advances in Understanding of Bluff Body Wakes and Vortex-Inducted Vibration*, pages 57–96, June 1998.
- [22] C. Norberg. Fluctuating lift on a circular cylinder: review and new measurements. *J. Fluids Struct.*, 17:57–96, 2003.
- [23] A. Papoulis. *Signal Analysis*. McGraw-Hill, 1984.
- [24] U. Piomelli. Large-eddy simulation: achievements and challenges. *Progress in Aerospace Sciences*, 35:335–362, 1999.
- [25] S. B. Pope. *Turbulent Flows*. Cambridge University Press, 2000.
- [26] Wolfgang Rodi. Large-eddy simulations of the flow past bluff bodies : State-of-the art. *JSME*, 41(2):361–374, 1998.
- [27] P. Sagaut. *Large eddy simulation for incompressible flows: An introduction*. Springer-Verlag, Berlin Heidelberg, third edition, 2006.
- [28] P. Sagaut, P. Comte, and F. Ducros. Filtered subgrid-scale models. *Physics of fluids*, 12(1):

- [29] L. Shao, S. Sarkar, and C. Pantano. On the relationship between the mean flow and subgrid stresses in large eddy simulation of turbulent shear flows. *Physics of Fluids*, 11(5):1229–1248, 1999.
- [30] J.S. Smagorinsky. General circulation experiments with the primitive equations: I. the basic experiment. *Mon. Weather Rev.*, 91:99–163, 1963.
- [31] S. Szepessy and P. W. Bearman. Aspect ration and end plate effects on vortex shedding from a circular cylinder. *J.Fluid Mech.*, 234:191–217, 1992.
- [32] H. Tennekes and J. L. Lumley. *A first course in turbulence*. MIT Press, 1972.
- [33] F. Toschi, H. Kobayashi, U. Piomelli, and G. Iaccarino. Backward-facing step calculations using the shear improved smagorinsky model. In *Proceedings of the Summer Program 2006, Center of Turbulent Research*, 2006.
- [34] S. Yokuda and B. R. Ramaprian. The dynamics of flow around a cylinder at subcritical reynolds numbers. *Phys. Fluids A*, 2(5):784–791, may 1990.
- [35] M. M. Zdravkovich. *Flow Around Circular Cylinders*. Oxford University Press, 2002.
- [36] This argument holds if neglecting non-commutation errors between the filter and partial derivatives.
- [37] Standard usage is to define the cut-off frequency at -3dB related to the attenuation of the power by half, and not of the amplitude. This would result in the removal of $\sqrt{3}$ in (9), therefore leading to the same order of magnitude for f_c . Here, we want to follow the convention commonly used in numerical simulations[17].
- [38] In the steady regime, the results in [14] using the Riccati equations for the Kalman filter show that the Kalman filter used here behaves as $[u]^{(n)} = (1 - \lambda) [u]^{(n-1)} + \lambda u^{(n)}$ for large times n . The smoothing factor λ is given by $\lambda = \overline{P}/(1 + \overline{P})$ with $\overline{P} = \lim_{n \rightarrow \infty} P(n|n-1) = q + \sqrt{q^2 + 4q}/2$ and $q = \sigma_{\delta[u]}^2/\sigma_{\delta u}^2$. In our physical context, $\lambda \ll 1$ and $\lambda \approx \sqrt{q} = \sigma_{\delta[u]}/\sigma_{\delta u}$. Hence, the rule proposed in the text.